Deformation and Flow of Red Blood Cells in a Synthetic Lattice: Evidence for an Active Cytoskeleton

James P. Brody,* Yuqi Han,* Robert H. Austin,* and Mark Bitensky‡
*Department of Physics, Princeton University, Princeton, New Jersey 08544; and ‡Los Alamos National Laboratory, Los Alamos, New Mexico 08570 USA

ABSTRACT We introduce the use of microfabrication techniques to construct on a silicon wafer a synthetic capillary bed with 2.5- to 4-micron (μ)-wide channels. Establishment of a fluid pressure gradient allowed us to observe simultaneously using optical microscopy hundreds of cells flowing through the bed at physiological speeds. We find a large distribution of mobilities among red cells flowing through the structure; smaller channels provide a greater impedance to flow than larger ones, indicating that kinetic drag variations provide the origin of the distribution. The mobility of a particular cell is not correlated with the cell diameter but appears to be inversely correlated with intracellular calcium concentration of the cell, as determined by fluorescence of the calcium-binding dye fluo-3 AM. Also, we are able to use the parallel processing nature of our arrays to observe isolated events where the rigidity of the red cell seems to change suddenly over several orders of magnitude as it blocks a channel in the array.

INTRODUCTION

There has been a longstanding mystery about the rate of ATP metabolism inside the red cell. Less than half of the ATP consumed can be associated with any specific processes (Weed, 1969). In other words, there is a very significant ATP-consuming process inside the red cell that remains unidentified. We believe that this process is a method by which the red cell can modify its rigidity. One can easily imagine scenarios where it is important for the red blood cell to be able to change rapidly its rigidity. For example, the mature red cell must go through a wide range of fluid flow conditions, from borderline turbulence in the aorta to low Reynolds and high shear flow in the capillaries. At high Reynolds numbers, it is important that the membrane be rigid and not be torn by large hydrodynamic forces, whereas in the capillaries it is important that the red blood cell maintain a highly deformable flexibility to pass through blood vessels as small as 4 μm in diameter (Whitmore, 1968). Thus, the cell has to be able to deform easily and yet still maintain its structural integrity. Because the average circulation time of a red blood cell in the body is about 1 min, this would imply that large and frequent changes in the membrane rigidity occur during circulation as the Reynolds number of the flow changes.

Because the minimum surface area enclosing a volume of fixed size is a sphere, the red cell with its biconcave shape has substantial excess surface area. The red cell has almost 50% more area than the equivalent sphere. This excess area is a key feature of its shape, because it allows the red cell to deform through openings smaller than its 8-μm diameter without tearing. A sphere, for instance, cannot deform at all if the volume and surface area is constrained to remain constant.

Thus, although the human red cell is often viewed as essentially a bag of hemoglobin that flows around the body, ferrying oxygen and carbon dioxide between individual cells and the lungs, there must be considerably more to the cell membrane structure and dynamics. The bag itself is composed of a membrane along with a cytoskeleton. The membrane is a thin, 100-Å wall composed of various biomolecules. The cytoskeleton is a mesh of spectrin molecules, a long, string-like protein. These molecules are linked together by other proteins, ankyrin and actin. The entire network is anchored to the membrane by a different protein, Band 3.1. The cytoskeleton sits on the inside of the membrane and gives the membrane a finite shear modulus.

In fact, the cytoskeleton is responsible for maintaining the red cell in its characteristic shape, a biconcave disc 8 μm in diameter and 2 μm thick at the thinnest part of the disk. That the cytoskeleton is quite active can be seen in how the cell can transform itself into different shapes depending on, among other things, the salt concentration in its environment (Miale, 1977). At high salt concentrations, it shrivels up into a form called an echinocyte, and at low salt it swells into a stomatocyte. The are several competing models for the underlying basis for these shape changes (Leibler, 1986) (Fisher, 1993) but there is general agreement that it is the cytoskeleton that plays the crucial role.

MATERIALS AND METHODS

This paper explores the hypothesis that hydrodynamic flow can induce changes in red blood cell membrane rigidity. We test this by constructing a device that forces red cells to deform repeatedly and quickly enough to pass through a 4-μ passage and return to their natural shape. This is to be distinguished from other experiments that deform the red blood cell statically by drawing into a micropipette tube, or pass the RBC through a single channel. This paper attempts to place the RBC into as close a replica as we can of its biological environment, in anticipation of unexpected responses of the RBC cytoskeleton to hydrodynamic flow.

Received for publication 23 September 1994 and in final form 6 January 1995.

Address reprint requests to Dr. Robert H. Austin, Department of Physics, Jadwin Hall, Princeton University, Princeton, NJ 08544-4353. Tel.: 609-258-4353; Fax: 609-258-1115; E-mail: rha@pupgg.princeton.edu.

0006-3495/95/06/2224/09 $2.00

Although single-cell pipette suction studies have been important sources of information concerning RBC deformability and elastic constants, pipette suction studies do not probe the dynamic behavior of the cytoskeleton of RBCs during fluid flow; nor do they allow the observation of large numbers of RBCs flowing through constrictive environments. Contrary to the pipette experiments, the RBC in our arrays is acted on effectively by a pressure head P due to hydrodynamic viscous fluid flow, not static suction.

Microfabrication of large obstacle arrays can be a powerful technique for studying many cells simultaneously, while still allowing one to isolate the small fraction of rigid cells. Measurements of transit times through filters have shown the presence of a small number of RBCs too rigid to pass through 5-μm-diameter pores (Koutsouris, 1988), but filters do not allow one to isolate the individual cells and ascertain their properties.

Design of the device

The design of the microfabricated flow chamber we constructed posed a number of interesting fluid dynamics questions. For instance, how much pressure was needed to induce a reasonable flow rate (10–100 μm/s) through a sparse matrix of channels of $\sim 4 \times 4\ \mu$ in cross section and 12 μ in length? A simple calculation gives an estimate.

An empirical fact discovered long ago (1856) is that for fluid flow at low Reynolds number in an isotropic media, the mean fluid velocity, $\bar{u}$, is proportional to the pressure gradient, ∇P (Batchelor, 1967):

$$-\nabla P = \frac{\eta \bar{u}}{k}, \tag{1}$$

where η is the viscosity of the fluid and k is a constant called the *permeability*, which is a function of the geometry through which the fluid is flowing. An intuitive way to view this equation is to associate the pressure gradient with a voltage and the mean velocity with a current; Eq. 1 is then seen to be equivalent to Ohm's Law, $V = IR$, if the "fluid resistance" is taken to be η/k.

We can calculate the approximate pressure needed to flow fluid through our microfabricated device by assuming a Hele-Shaw cell geometry (ignoring all the rectangular blocks) and setting $k = h^2/12$ (Kadanoff, 1986) (calculated analytically), where h is the distance between the two surfaces,

$$-\nabla P = \frac{12\eta \bar{u}}{h^2}. \tag{2}$$

For a 4-μ spacing between plates, we would need a pressure gradient of $\sim 10^{-2}$ psi/cm to get flow of water at 10 μ/s.

Another way to estimate this is to assume flow in a long circular tube with a fixed pressure gradient (Poiseuille flow). Poiseuille's solution to this problem is usually written in the form:

$$-\nabla P = \frac{8\eta\pi Q}{R^4}, \tag{3}$$

but because we are interested in the average fluid velocity, $\bar{u}$, and not the volume flow rate, Q, we rewrite the equation in terms of $\bar{u}$,

$$-\nabla P = \frac{8\eta\pi^2 \bar{u}}{R^2}, \tag{4}$$

where R is the pipe radius, and we get numbers about 3 times higher for the pressure than we did for the Hele-Shaw geometry. It turns out, because of the complex geometry that we use, that we need about twice as large a pressure drop across the microfabricated arrays as we would for Hele-Shaw geometry. This means that the fluid resistance is about twice as large.

The total length across which our external pressure drop occurred was 2 cm, and there is a narrow channel every 25 μ, so we estimate that if an external pressure P_o is applied to the array the pressure head P of each channel is $25/(2 \times 10^4) = 1.2 \times 10^{-3} P_o$. This is quite a small number, and of importance later in this paper as we study the minimum pressure needed to buckle the cell.

The fluid dynamics inside the sealed array is always laminar. This can be quantified by the Reynolds number, which is just the ratio of the inertial to the viscous terms of the Navier-Stokes equation:

$$R_e = \frac{\rho l u}{\eta}. \tag{5}$$

For fluid flow through microstructures studied in this work, some typical values are flowing water, u = 1–100 μm/s and l = 10 μm. This gives a typical $R_e = 10^{-3}$ to 10^{-5}. Turbulence is a complex process but usually will not occur at Reynolds numbers less than about 10^3, and certainly never below 10^0. So the flow should be laminar and smooth at all times, and complex phenomena such as vortex formation cannot occur. To confirm this, fluid flow patterns were recorded by imaging the fluorescence of balls with an integrating digital 1024 × 1024 CCD camera (Hamamatsu C-4880) and fluorescent polystyrene balls from Duke Scientific (data not shown). Balls of diameter 0.1 μ were used for these measurements. No turbulence or secondary flows were present. All flow was strictly smooth laminar flow, with no back-flow or vortices, as expected.

Construction of the sealed array

We used silicon processing techniques at the National Nanofabrication Facility (Cornell University, Ithaca, NY) to fabricate a large, sealed array of capillary sized channels on 3" silicon wafers. Two different arrays were constructed for these experiments. The simplest array consisted of channels of length 12 μ was followed by an open length of 13 μ. The etch depth was set at 4.0 μ, as shown in Fig. 1, using a process detailed in Table 1 (Chinn, 1981).

Scanning electron micrographs showed a surface roughness of <100 Å. The second array was constructed with variable width channels: Fig. 1 *A* shows a scanning electron microscope (SEM) image of a section of a multi-width array. This array has parallel sections where the channel width was varied from 2.5 to 4.0 μ in 0.5-μ steps. Note the microscopic smoothness of the walls of the array and the uniformity of the environment from channel to channel: all of the channels are identical. This array was used to determine whether the channel-opening area influences the cell mobility when normalized by the fluid flow velocity.

Sealing of the arrays is a critical step. Pyrex coverglass was ordered from Esco Products (Oak Ridge, NJ). The glass was scribed and cut to size. A hole ~1/16" in diameter was ground through the glass using a diamond-tipped, cone-shaped bit (Wale Apparatus Co., Hellertown, PA) on a high speed (21,000 rpm) drill. The glass was washed carefully with Micro detergent and water to remove any bits of diamond and glass. The glass was attached to the silicon device using anodic bonding (Wallis, 1969) (Brody, 1994). The glass was held at −400 V with respect to the silicon for 60 min while being heated to 400°C. The glass was placed so that it sealed around the etched area on three sides. Fig. 1 *B* gives a sketch of a completed sealed variable width array. A 1/8" (ID) glass tube was epoxied around the hole in the coverslip, and the flow rate was controlled by varying the tube pressure relative to atmospheric pressure from -10^5 to $+10^6$ dyn/cm^2 (−0.1 to +1.0 bar).

Experimental protocol

Fresh blood was drawn from M. Bitensky or J. P. Brody and promptly diluted ~100:1 in Ringers buffer containing 1 mM heparin to minimize sticking of the RBCs to the internal structure of the array. We estimate the final hematocrit inside the array at between 0.1 and 0.01%. All experiments were done at 20°C. Video of individual RBCs was recorded through a Nikon Optiphot 2 microscope taken with either a monochrome CCD video camera (Panasonic GP MF-502) or a photon-counting camera (Hamamatsu C2400–47) onto a S-VHS VCR (Mitsubishi BV-1000 or Mitsubishi U82). Video from the VCR was digitized by a frame-grabber (Dipix 3360F) and processed on an PC clone using commercial image-processing software (Optimas, BioScan Inc., Edmons, WA).

Calcium measurements were made using the indicator dye fluo-3 AM. (Molecular Probes, Eugene, OR). This was dissolved in a stock solution of 1 mM DMSO and diluted to a final concentration of 1 μM in Ringers buffer. Freshly drawn blood was diluted 100:1 in this buffer and incubated for 0.5

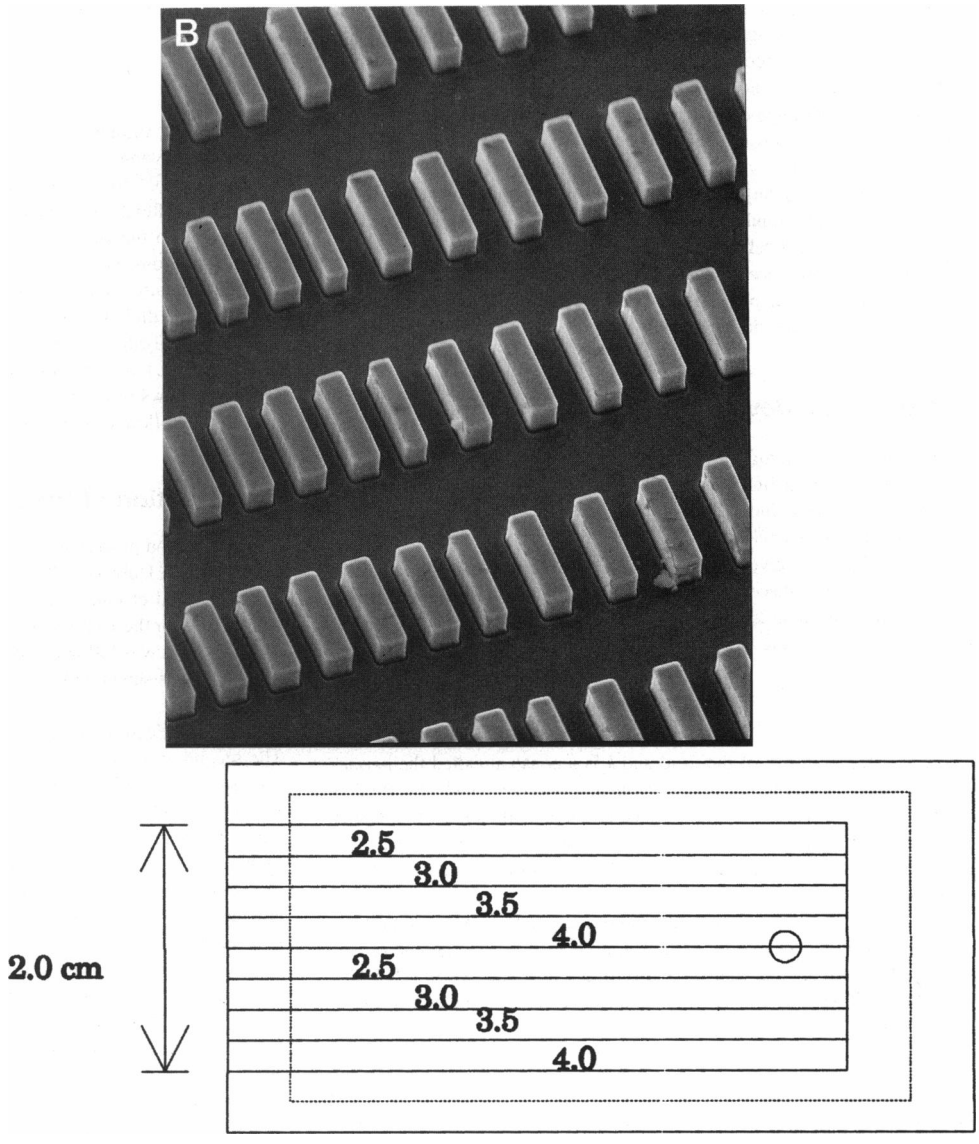

FIGURE 1 (*A*) Electron microphotograph of an array containing four different channel widths (2.5, 3.0, 3.5, and 4 μ). The channels where 20 μ in length and can be used as the length bar for this figure. The scanning electron microscope image shows the boundary between 4.0 μ width slot (*right*) and 2.5 μ width slot (*left*) sections. (*B*) Schematic diagram of the completed chip showing the pressurizing tube, sealed array, edge where RBC suspension is applied, and the general region of microscopic observation on the left-hand side of the sealed chip where the flow is closely parallel to the channels. The numbers running from 2.5 to 4.0 represent the width in the parallel sections of channels in μ. The dashed rectangle shows the coverage of the Pyrex coverslip. The circle at the right-hand side of the sealed region represents the hole drilled in the Pyrex coverglass slide through which fluids were applied at positive or negative pressure relative to atmospheric pressure. Red blood cell suspensions were applied to the left-hand side, where microscopic observations were made.

h at 20°C. The RBCs were then washed 3 times in Ringers buffer (free of fluo-3 AM) to remove any dye that had not diffused into the cells. Cell luminance was determined by the following protocol. The cell outline was traced using the software package Optimas. The integrated luminance (integrated intensity) of the cell image was subtracted from a background level obtained by moving the cell outline over to an adjacent dark region to determine the background luminance. Background luminance was also used to correct for slow variations in the illumination field intensity by dividing the (cell background) luminance by the background luminance.

RESULTS

Shape of deformed RBCs

Fig. 2 shows a video time sequence of a RBC passing through a 4-μ-width channel. Note that upon leaving the channel the RBC elastically returns to its undeformed shape. The time between the frames in Fig. 2 is 0.2 s, giving an average speed of ~20 μ/s for the cell at a pressure gradient of 2×10^4 dyn/cm^3 (0.30 lb/in^3), or a channel pressure head $P = 25$ dyn/cm^2. At this low flow rate, the cells typically fold like a hot-dog bun, whereas at higher flow rates the thin center of the RBC migrates to the rear of the cell (Brody, 1994) (data not shown).

Distribution of mean speeds

We found that there exists a large dispersion in RBC speeds. The dispersion in the cell speeds arises when the cells are inside the narrow channels and not when they enter the channel (see below). Fig. 3 presents histograms of cell mobilities corrected for fluid flow speeds. Normalization was accomplished by tracking 0.1-μ balls through the channels and determining their average speed in the channel, then dividing a particular cell speed through the channel by the bead speed. Fig. 3 shows that in fact RBCs have lower mobility in the narrow channels than the wide channels. Koutsouris et al. (1988) also saw distributions in cell transit times using electrical conductance changes, but their distribution function is considerably more skewed to long transit times than ours,

TABLE 1 Silicon processing at the National Nanofabrication Facility

Process Step*	Notes
Vapor prime	HMDS (hexamethyldisilazine) process adhesion promoter
Resist coating	Shipley 805 positive resist Prebake 115°C for 30 s on vacuum hotplate Spin on at 4000 rpm for 30 s Gives 0.5-micron coating
Expose	Nominal time 0.1 s at g-line (436 nm)
Develop	Shipley MF-321 for 1 min, gentle agitation rinse in deionized water
SiO_2 etch	30 scc/m ChF_3, 30 mTorr, 0.25 W/cm^2 Flow O_2 at 1.0 scc/m to burn off resist slowly Etches SiO_2 at 300Å/min 2:1 selectivity with photoresist mask
Si etch	(1) Remove water on surface at −200 V and 20 mTorr, flow BCl_3 14 scc/min H_2 7 scc/min for 1 min (2) Remove native oxide at −300 V and 20 mTorr, flow Cl_2 2 scc/min BCl_3 14 scc/min H_2 7 scc/min for 1 min (3) Etch silicon at −400 V and 40 mTorr, flow Cl_2 50 scc/min BCl_3 5 scc/min Etches silicon at 1600 Å/min 12:1 selectivity over SiO_2 mask Remove wafer and rinse in deionized water

*From Chinn (1981).

which is roughly Gaussian in shape. At this point, we do not know whether the distribution function is strongly sensitive to the materials used to construct the channels. Because Koutsouris et al. are not able to observe individual cells optically, the possibility exists that their skewed distribution function originates from cells "sticking" to the structure and then pulling away rather then true kinetic effects.

Channel width influences the cell mobilities, but does not change qualitatively the form of the distribution function. Fig. 3 *B* shows the normalized cell mobilities in the channels for 4.0- and 2.5-μ-wide channels. The cells show greater retardation in the narrower channels.

Because in our array we are able to observe all of the cells simultaneously, we were able to look for correlations between the cell morphology and mobility. The most obvious correlation to look for is one between mobility and cell diameter, diameter also being a distributed function in a unfractionated cell population. Cell diameters were determined by grabbing video frames and using the software image analysis program Optimas (BioScan) to determine cell diameters. Cell diameters can be determined with an accuracy of $\sim\pm0.25$ μ. Fig. 4 indicates that there is no correlation between cell speed and. A Pearson linear correlation analysis done using the statistical analysis package Systat (Systat Inc., Evanston, IL) between the cell diameter and speed yields a correlation coefficient of −0.101, showing no effective correlation.

The presence of channel width-dependent mobility distributions uncorrelated with diameter reveals that there are variables controlling cell mobility in addition to RBC diameter that have a large variance in a given RBC population.

The biconcave shape of the RBCs, maintained by a cortical cytoskeleton, has a 50% excess surface/volume ratio at physiological salt concentrations compared with a sphere of the same volume. This excess surface area makes it geometrically possible to have iso-volume deformation of the RBC as it goes through any of our channels (Kowluru, 1989), and the elastic deformation of the surface can play a role in the mobility of the RBC at a given pressure head.

The elastic energy cost of the required deformation can be analyzed via the known material properties of the red cell, which have been well characterized in the past on an individual basis by pipette suction techniques (Evans, 1973, 1979). Because the membrane is so thin (100 Å), the entry of the RBC into the channel is viewed best as a buckling phenomena.

Evans (1983) has shown that the critical buckling pressure $P_c \sim 2B/R_p^3$, where B is the membrane-bending modulus and R_p is the radius of the channel. The bending modulus B arrived at from pipette suction experiments is $\sim 1.8 \times 10^{-12}$ dyn/cm; thus, RBCs will buckle into 4-μ-diameter holes for pressure heads $>\sim 0.5$ dyn/cm^2, considerably less than our pressure head of ~ 20 dyn/cm^2.

Because pressure drop is always well above the buckling threshold, it would seem that even wide variations in bending rigidity would imply constant (near zero) entry time for a population of RBCs into a 4-μ-wide channel. However, we see wide variations in RBC mobility. Therefore, kinetic friction between the cell membrane and the native silicon dioxide surface of the narrow channel would seem to be the logical choice as the main variable governing the dispersion in mobilities. Qualitative observations confirm this. The difference between "fast" RBCs and "slow" RBCs clearly occurs when the cell is entirely folded into the channel. "Fast" and "slow" RBCs travel at the same speeds between channels and entering channels.

The kinetic friction can be broken down into two variables. For example, deformation of a RBC will result in a normal force N exerted against the channel wall due to the stress applied to the cell membrane, and a retarding frictional force $F_f = \kappa N$ characterized by the kinetic frictional coefficient, κ. An increase in the membrane-bending modulus B and/or a decrease in the radius of curvature R will increase the normal force, N. Narrow channels will exert greater normal forces on the cell than wide channels because of the smaller radius of curvature, and this should decrease the average speed, as we show in Fig. 3.

Fluorescence measurements

It is also possible to examine whether the distribution in mobilities is due to a distribution in RBC membrane-bending rigidity, B, or a distribution in the coefficient of friction, κ. Weed and Lacelle (1969) have shown that introduction of

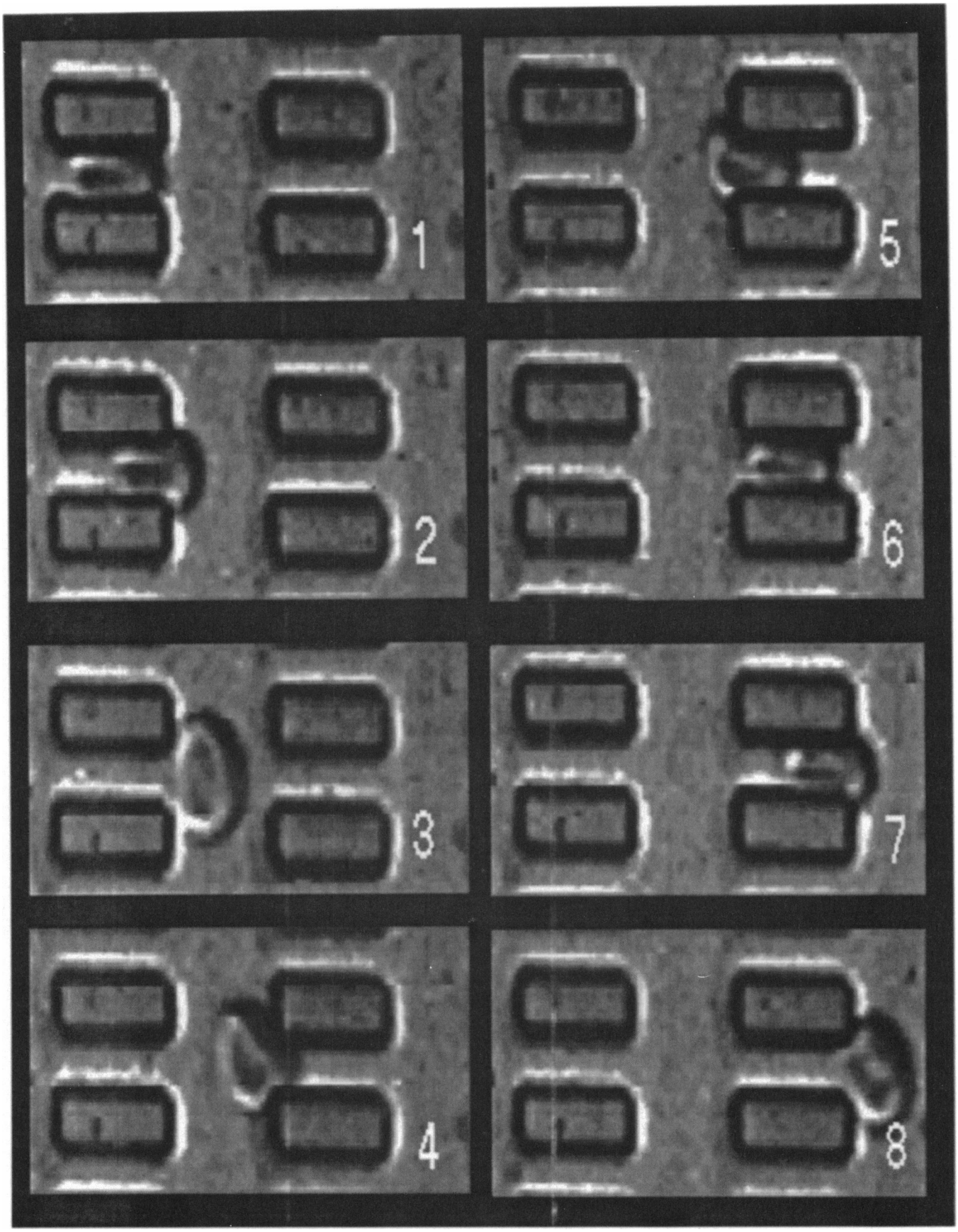

FIGURE 2 Video frames of an RBC flowing through a 4-μ width channel. Electronic camera shutter speed was set at 10^{-3} s; the frames numbered 1 through 8 are 0.2 s apart.

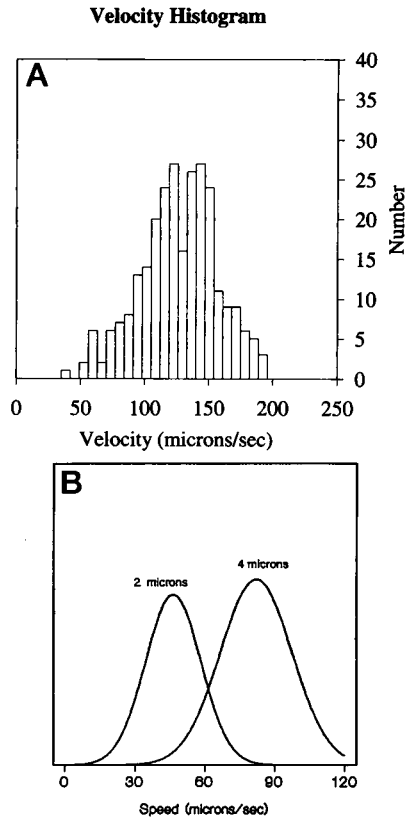

FIGURE 3 (*A*) Histogram of the average cell velocities in a 4-μ width channel, 4-μ etch depth in a pressure gradient of $\sim 10^5$ dyn/cm^2. The average RBC speed as determined by the time it takes to traverse 200 μ. (*B*) Histogram of average cell velocities in channels of width 4 and 2.5 μ in a pressure gradient of $\sim 10^5$ dyn/cm^2. The etch depth is 4 μ in both cases and was compensated by changes in fluid speed in the differing areas by dividing by the average speed of 0.1-μ balls moving through the section. Gaussian fits are shown as solid lines.

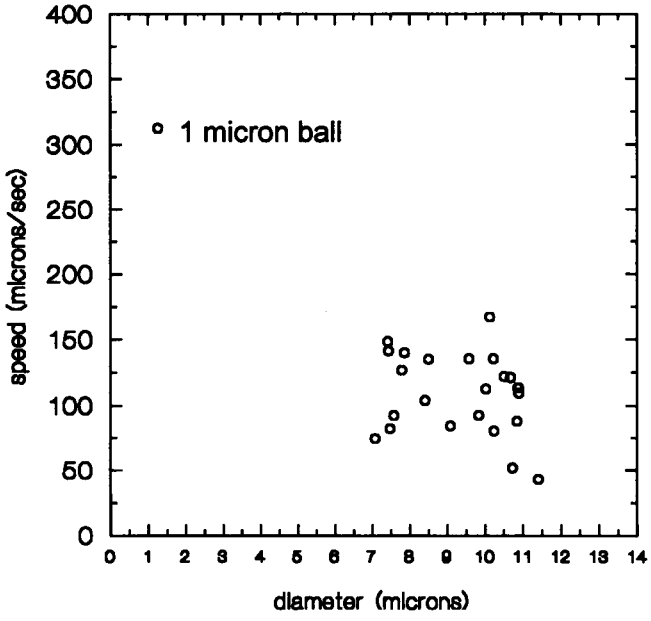

FIGURE 4 Average cell speed versus observed cell diameter with a pressure gradient of $\sim 1.5 \times 10^5$ dyn/cm^2. The cell diameters were determined in the open areas between the channels by frame-grabbing a video imaging and fitting the cell to a circular shape. Cell diameters can be determined with an accuracy of $\sim \pm 0.25$ μ. The point in the upper left-hand quadrant labeled "1 μ ball" is the speed 1-μ-diameter polystyrene balls at this pressure gradient.

excess calcium into RBCs can increase the bending modulus 90-fold, indicating that the actin/spectrin system of the cytoskeleton may be activated by calcium. A possible triggering mechanism for the effects that we have seen is that shear forces trigger calcium gates (Larsen, 1981) that activate the actin/spectrin network (Schrier, 1981) and greatly increase the cortical cytoskeleton rigidity. An indirect test of membrane rigidity modulation is real-time measurements of intracellular calcium levels.

We have carried out real-time video microscopy of the fluorescence intensity of RBCs that have been incubated with the calcium-binding dye fluo-3 AM (Molecular Probes), a fluorescent dye that is activated upon passage through the RBC membrane and subsequent hydrolysis of the acetoxymethyl group (Minta, 1989). The very high speed response and high quantum yield of the Hamamatsu camera's phosphor (<1/30 s decay time) allowed us to monitor the temporal variations of the intra-calcium levels in the RBC as it passed through the array. Fig. 5 shows a series of three fluorescence images for two cells (a slow and a fast one) passing through a series of channels. Two facts are evident from these frames: there appears to be an inverse correlation between RBC intracellular Ca^{2+} concentration, and there are substantial variations in the Ca^{2+} concentration as the RBCs move through the array. Fig. 6 is a plot of observed RBC fluorescence intensities as a function of speed, and it makes this point clear. A Pearson linear correlation analysis between the normalized brightness and the speed of the cells through the channels supports this hypothesis: the correlation coefficient is −0.771. Although there is a clear correlation between speed (mobility) and cell fluorescence, there is substantial variability from cell to cell.

Rigid cells

A final feature of the arrays is that they allow us to pick out unusual cells from a large population of "normal" cells, and we have been able to observe even more dramatic effects indicating that the cell rigidity can vary greatly with time and can exceed the critical buckling value. Fig. 7 is taken from a series of video frames of a cell progressively slowing and stopping in a 4-μ-wide channel even though the flow speed is such that "normal cells" move through the array at speeds of over 400 μ/s. The cell completely stops within the channel at position 165 μ. Fig. 8 shows the cell in the subsequent 30 s after stoppage: note that even in the presence of a fluid velocity flow of 400 μ/s or a pressure head P of 500 dyn/cm^2 that the cell proceeds to back out *against* the flow by assuming a cylindrical shape. Approximately 10 s after the last frame shown here, the cell spontaneously buckled and proceeded to flow at high speed through the channels.

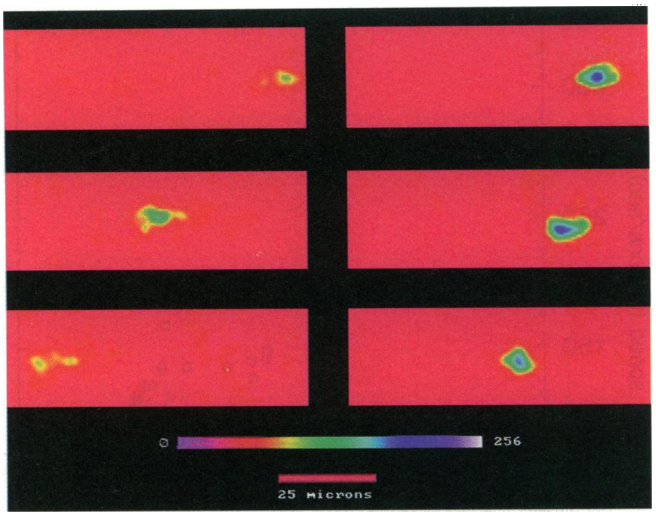

FIGURE 5 False-color fluorescence image of two different cells moving through a common array area. The time between frames is 0.5 s. There is no smearing of the image in this photo because the phosphor decay time of the camera is under 1/30 of a second.

We have observed that ~1 cell in 1000 at any one time transiently blocks a channel. All cells eventually buckle and continue to move. Blocked cells often are hit almost head-on with a cell moving at the normal 400 μ/s speed, and Fig. 9 shows a fortuitously grabbed frame of such an event. Note that the rapidly moving cell on the right is highly deformed by the collision, whereas the "rigid" cell shows no deformation! This indicates conclusively that although friction is the means by which rigidity influences mobility, the stopped cell did have a very high rigidity, indeed, because it did not deform appreciably in the collision. A rough estimate of the stopped RBC's time varying shear modulus can be found from the formula for the fractional intrusion length $x = L/R_p$ of a RBC into a channel of radius $R_p > L$ in the presence of

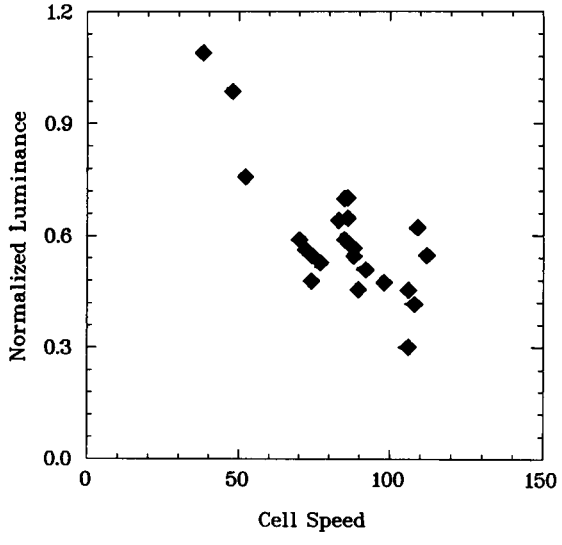

FIGURE 6 Observed cell luminance versus cell velocity. The method by which the corrected cell luminance was determined is described in the text.

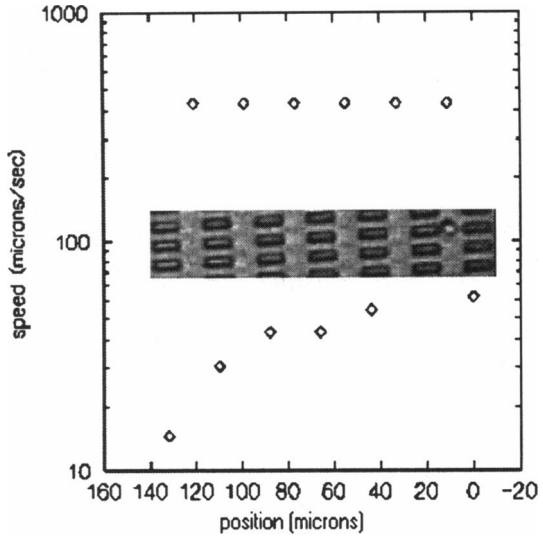

FIGURE 7 Speed of a cell as it slowed down in a series of channels of 4-μ width. The speed was determined by frame-grabbing successive video images and determining the distance traveled between frames. A microphotograph strip of the channels is shown in the plot to indicate the cell position in the graph. Note that the speed of the cell moving through unconstricted part of the array was 400 μ/s. The small circle in the photomicrograph strip is a RBC between channels.

a pressure head P (Chien, 1987):

$$\mu = R_p P[1 + x^2]/[2x(\ln(1 + x^2) + x^2)]. \quad (6)$$

Inspection of the L/R_p in Fig. 9 shows that μ seems to achieve values of up to 20 dyn/cm, compared with the typical value of $\sim 10^{-2}$ dyn/cm derived from pipette suction experiments.

CONCLUSIONS

We have presented evidence for strong cell-to-cell variations in membrane rigidity and for striking cases where the cell membrane can increase rigidity by at least several orders of magnitude. There seems to be a good correlation between cell mobility and internal calcium concentration, as ascertained by fluor-3 CM fluorescence measurements. All of these effects call into play a strong involvement of the cytoskeleton and membrane rigidity. It has been shown by several computer simulations (Leibler and Maggs, 1990; Boal, 1994) that the spectrin network can both explain the shape of RBC's and that variations in the connectivity of the spectrin network can strongly influence the effective bending and shear moduli of the network, over several orders of magnitude. Such a dramatic increase in rigidity is need to explain the "rigid" cells observed in this work. Because spectrin connectivity is driven by calcium ions, it seems to make sense that the variations in rigidity observed here are correlated with the calcium ion concentration within the cell.

These are still simple and naive experiments. Despite the seeming simplicity of the RBC, there clearly exist important unresolved issues concerning RBC elastic properties, their

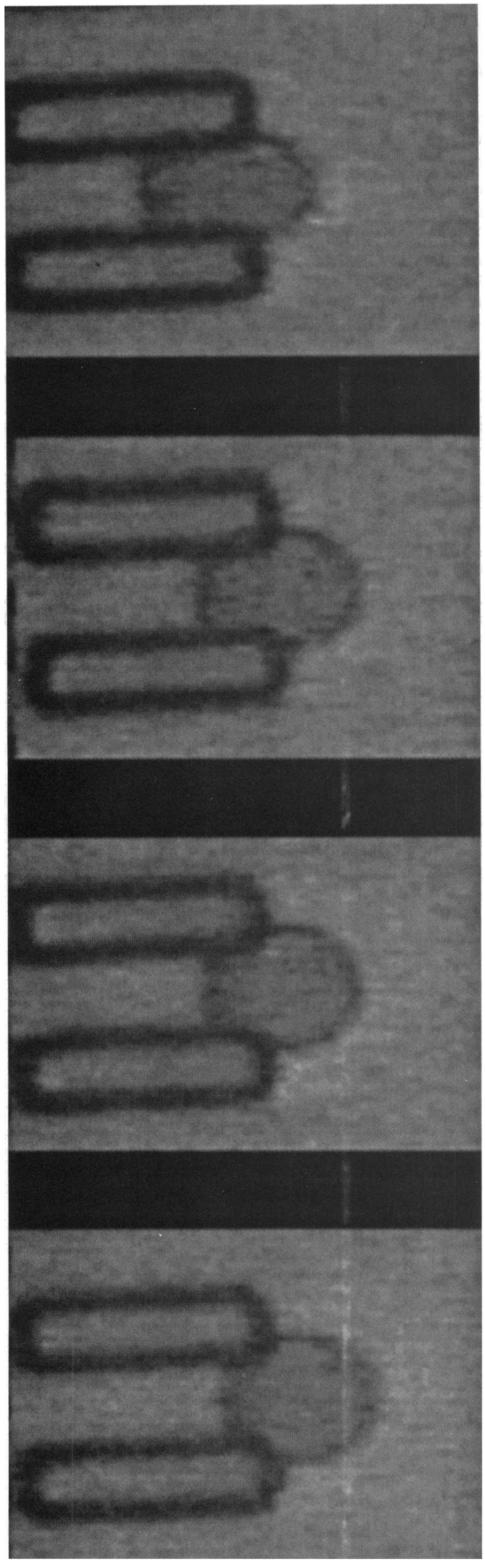

FIGURE 8 Images of the same cell in Fig. 7 after stopping within a channel. Fluid flow is to *left*, velocity 400 μ/s. The the cell backs out *against* the flow. The time between images here is 10 s.

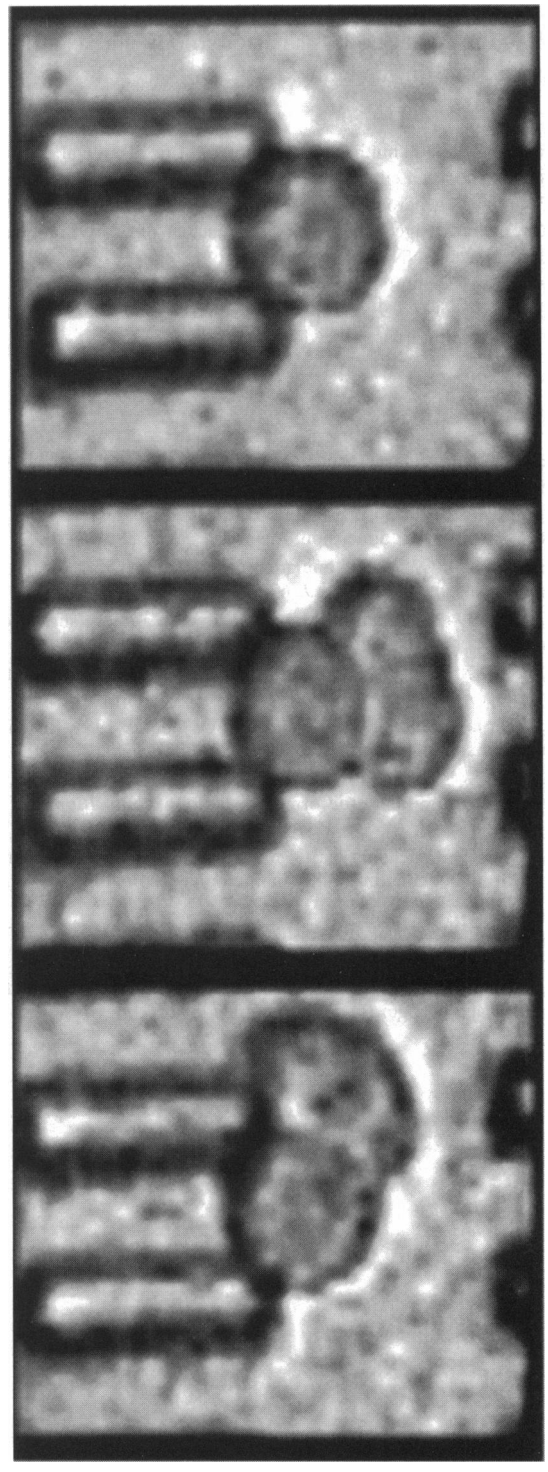

FIGURE 9 Cell moving at 400 μ/s colliding with the cell in Fig. 3 *A* at the point where it had nearly completely backed out of the channel. The camera shutter speed was set electronically at 10^{-3} s. Note the high deformation of the cell moving from the right and the undeformed circularity of the rigid cell.

time dependence, and biological significance. Recent experiments by Evans et al. (1994) have indicated dramatically the degree to which the RBC membrane can change its rigidity. This paper demonstrates the power of microfabricated en-

vironments to probe the variability of cell elastic properties, which is important both for basic biology and as a possible diagnostic tool in medicine.

We thank Wayne Volkmuth, F. P. Camilo, Ted Cox, Tom Duke, Raymond Goldstein, Stanislas Leibler and Watt W. Webb for helpful discussions. Dave Vaniman's generous use of his microscope and facilities at LANL is gratefully acknowledged, and the expert assistance of Garry Bordonaro and Rich Tiberio at the NNF.

This work was supported by National Science Foundation grant MCB-9202170, Office of Naval Research grant N00014–91-J-4084, and National Institutes of Health grant 1 R03 RR08032-01.

REFERENCES

Batchelor, G. K. An Introduction to Fluid Dynamics. Cambridge University Press, Cambridge, MA.

Bensimon, D., L. Kadanoff, S. Liang, B. I. Shraiman, and C. Tang. 1986. Viscous flow in two dimension. *Rev. Mod. Phys.* 58:977–999.

Boal, D. H. 1994. Computer simulation of a model network for the erythrocyte cytoskeleton. *Biophys. J.* 67:521–529.

Brody, J. P. 1994. Fluid and cell transport through a microfabricated flow chamber. Ph.D. thesis. Princeton University, Princeton, NJ.

Chien, S. 1987. Red cell deformability, and its relevance to blood flow. *Annu. Rev. Physiol.* 49:177–192.

Chinn, J. D., I. Adesida, E. D. Wolf, and R. C. Tiberio. 1981. Reactive ion etching for submicron structures. *J. Vac. Sci. Technol.* 19:1418–1422.

Evans, E. 1973. New membrane concept applied to the analysis of fluid shear, and micropipette-deformed red blood cells. *Biophys. J.* 13: 941–954.

Evans, E. A. 1983. Bending elastic modulus of red blood cell membrane derived from buckling instability in micropipet aspiration tests. *Biophys. J.* 43:27–30.

Evans, E. A., and R. Skalak. 1979. Mechanics and thermodynamics of membranes. I. *Crit. Rev. Bioeng.* 3:180–330.

Fisher, T. M. 1993. Bending stiffness of lipid bilayers. IV. Interpretation of red cell shape change. *Biophys. J.* 65:687–692.

Knowles, D. W., J. A. Chasis, E. A. Evans, and N. Mohandas. 1994. Cooperative action between band 3 and glycophorin A in human erythrocytes: immobilization of band 3 induced by antibodies to glycophorin A. *Biophys. J.* 66:1726–1732.

Koutsouris, D., R. Guillet, J. C. Lelievre, M. T. Guillemin, P. Bertholom, and M. Boynard. 1988. Determination of erythrocyte transit times through micropores. I. Basic operational principles. *Biorheology.* 25:763–772.

Koutsouris, D., R. Guillet, R. B. Wenby, and H. J. Meiselman. 1988. Determination of erythrocyte transit times through micropores II. influence of experimental, and physicochemical factors. *Biorheology.* 25:773–790.

Kowluru, R., M. W. Bitensky, A. Kowluru, M. Dembo, P. A. Keaton, and T. Buican. 1989. Reversible sodium pump defect, and swelling in the diabetic rat erythrocyte: effects on filterability, and implications for microangiopath. *Proc. Natl. Acad. Sci.* 86:3327–3331.

Larsen, F. L., S. Katz, B. D. Roufogalis, and D. E. Brooks. 1981. Physiological shear stresses enhance the Ca^{2+} permeability of human erythrocytes. *Nature.* 294:667–668.

Leibler, S. 1986. Curvature instability in membranes *J. Physique.* 47: 507–516.

Leibler, S., and A. C. Maggs. 1990. Simulation of shape changes, and adhesion phenomena in an elastic model of erythrocytes. *Proc. Natl. Acad. Sci. USA.* 87:6433–6435.

Miale, J. B. 1977. Laboratory Medicine: Hematology. C. V. Mosby, St. Louis. 549–605.

Minta, A., J. P. Y. Kao, and R. Y. Tsien. 1989. Fluorescent indicators for cytosolic calcium based on rhodamine, and fluorescein chromophores. *J. Biol. Chem.* 264:8171–8178.

Schrier, S. L., B. Hardy, I. Junga, and L. Ma. 1981. Actin-activated ATPase in human red cell membranes. *Blood.* 58:953–962.

Vogel, S. 1992. Vital Circuits. Oxford University Press, New York.

Wallis, G., and D. I. Pomerantz. 1969. Field-assisted glass-metal sealing. *J. Appl. Phys.* 40:3946–3949.

Weed, R. I., and P. L. Lacelle. 1969. ATP dependence of erythrocyte membrane deformability. *In* Red Cell Membranes: Structure and Function. Lippincott, Philadelphia. 318–338.

Whitmore, R. L. 1968. Rheology of the Circulation. Permagon Press, New York.